www.czasopisma.pan.pl PAN POLSKA AKADEMIA NAUK www.journals.pan.pl

Arch. Min. Sci. **71** (2026), 1, 17-34

Electronic version (in color) of this paper is available: http://mining.archives.pl

DOI: https://doi.org/10.24425/ams.2026.157754

IVÁN GONZÁLEZ PÉREZ[1*], ENOC SANZ ABLANEDO[1], JOSÉ RAMÓN RODRÍGUEZ PÉREZ[1]

MONITORING VOLUMETRIC CHANGES IN MINING WASTE-DUMPS USING VERY HIGH-RESOLUTION SATELLITE IMAGERY, IN-SITU GNSS DATA, AND SFM UAV DATA FUSION

Accurate volumetric estimation of mining waste-dumps is crucial for cost management and environmental monitoring. In this study of an active marble quarry, we evaluated the accuracy and reliability of digital elevation models (DEMs) derived from two very high-resolution (VHR) satellites – Pléiades Neo (PleN) tri-stereo and WorldView-2 (WV2) – compared to a reliable high-precision UAV-based model. Recording for the three DEMs was performed by extracting 30 secondary ground control points that were easily recognizable in the different DEMs. Evaluation involved the selection of stable control plots, where no surface changes were apparent in visual inspection. For these control areas, we evaluated the altimetric differences of the satellite-derived DEMs compared to the UAV DEM, finding that PleN and WV2 yielded mean vertical offsets of –11.7 cm and –18.6 cm (root mean square errors of 24.8 cm and 20.7 cm), respectively. Our findings underscore the potential of VHR satellite imagery for the evaluation of mining waste volumes and provide guidelines for optimal georeferencing and recording of periodically generated DEMs using UAV-derived DEMs obtained at specific points in time.

Keywords: Photogrammetry; mining waste-dump; VHR satellite imagery; terrain digital reconstruction

1. Introduction

The mining industry, in playing a crucial supply role for energy and raw materials, holds a key position in the global economy. However, its operations also present significant environmental and social challenges that must be carefully managed. The rising demand for mining resources has led to the accumulation of large volumes of mining waste, posing serious environmental risks [1]. These risks include soil and water contamination, fertile land erosion, landscape degradation, and substantial visual impacts [2-4]. Addressing these issues is essential to ensuring the long-term sustainability of the mining sector.

[1] UNIVERSIDAD DE LEÓN, SPAIN

* Corresponding author: igonp@unileon.es

In this context, accurately quantifying earth movements is crucial, as compliance with waste management policies requires records of the surface of the extraction site and the amount and type of waste [5]. Having available rapid and reliable tools for continuously monitoring a mine's topography is extremely beneficial, as this enables real-time decision-making and enhances the overall efficiency, safety, and environmental sustainability of operations [6-7]. Monitoring can be done through terrain surveys and 3D models, which can be used to calculate the volume of deposed material [8]. Digital elevation models (DEMs) are essential for tasks such as estimating waste-dump volumes and monitoring extraction operations [9].

Traditionally, volume measurements are carried out by specialist technicians, who are required to conduct substantial fieldwork in often difficult environmental conditions; when the surface area is very large, an aircraft photogrammetric flight is often commissioned. However, this approach is inefficient in terms of both time and data results, and moreover, the financial and logistical costs are significant [10-11]. The emergence of unmanned aerial vehicles (UAVs), i.e., drones, has opened up a whole new perspective, and in recent years their use in combination with photogrammetric techniques, e.g., the structure-from-motion (SfM) approach [12] has increased in remote sensing research [13]. This technology is appealing given its ability to capture data at a low cost and with high spatial and temporal resolution, possibly even yielding greater accuracy and detail than terrestrial geodesic measurements [14-15]. Numerous studies across various knowledge fields, such as flood risk assessment, construction, agriculture, and mining, have employed drones to generate DEMs with satisfactory results [16-19].

With the emergence of very high-resolution (VHR) satellites such as IKONOS, GeoEye-1, Pléiades Neo (PleN), and WorldView-2 (WV2), satellite imagery has become increasingly important for photogrammetric applications, with VHR image (<1 m pixel) archives having grown exponentially in the past decade [20]. The rapidity of data acquisition and the large surface area covered by VHR satellite images make for applications that are both cost effective and efficient [21], as evidenced by the growing number of studies that employ these images to generate DEMs [22-24]. However, the precision and accuracy of satellite-derived DEMs is still debated. Loghin et al. [25] examined the vertical accuracy of Pléiades tri-stereo and WorldView-3 (WV3) DEMs compared to the light-detection-and-ranging (LiDAR) technology in open, vegetation-free areas, achieving root mean square error (RMSE) values of 0.96 m and 0.37 m, respectively. Similarly, Zhou et al. [26], on comparing Pléiades tri-stereo to LiDAR, obtained vertical accuracy of 0.3 m. While these results are undoubtedly positive, in that they highlight the remarkable potential of this technology, they have not yet led to VHR satellite imagery becoming the standard for DEM generation. Data processing challenges persist, along with concerns regarding the consistency of georeferencing across images from different dates or sources.

The primary objective of our study was to assess the effectiveness of combining VHR satellite imagery from different dates and sources, in-situ Global Navigation Satellite System (GNSS) data collection, and high-resolution UAV imagery to periodically monitor volumetric changes in a mining waste-dump.

2. Material and methods

The methodological workflow for this study is described in Fig. 1. The process began with fieldwork, which included several land surveys – aimed at collecting ground control point (GCP) data – and five UAV photogrammetric flights. The surveys were conducted around the same

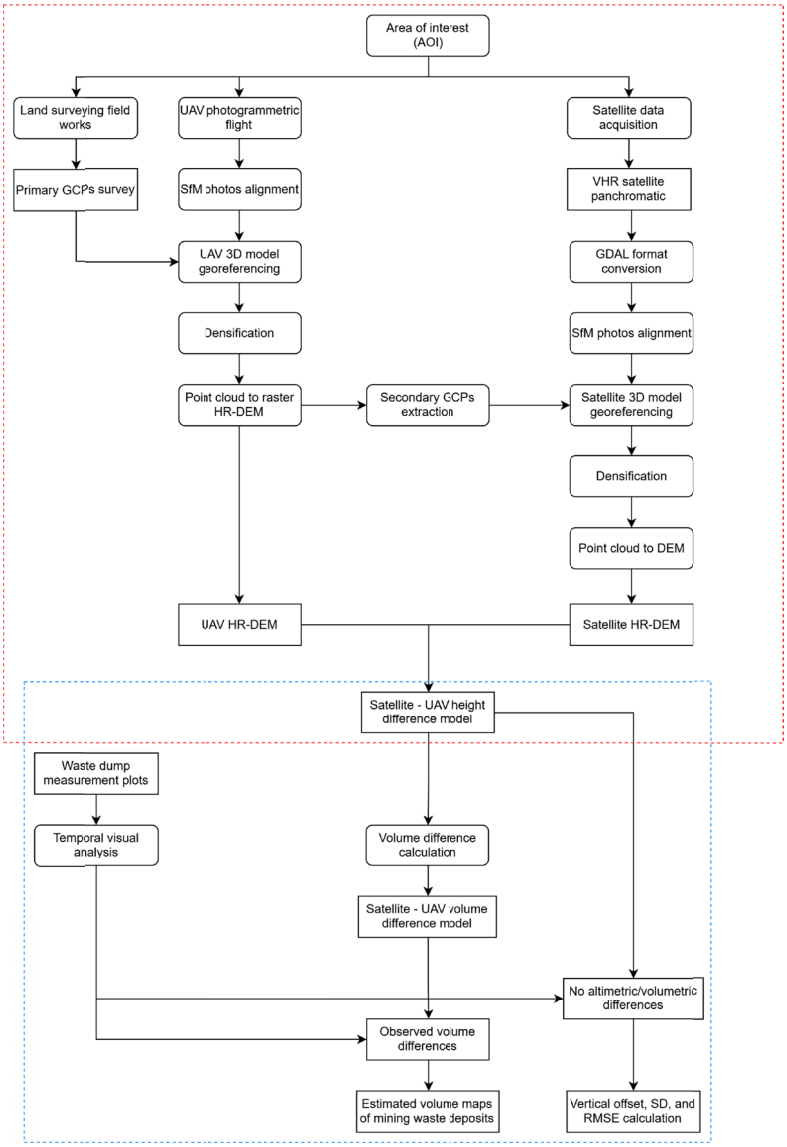

Fig. 1. Study methodology workflow. The red-dashed box indicates the workflow of the proposed approach to periodically generate digital elevation models (DEMs) with very high-resolution (VHR) satellite imagery. The blue-dashed box outlines the workflow for the results validation process

time as the acquisition of PleN tri-stereo images, while the stereo WV2 images were acquired six months later.

Using the UAV imagery and the collected GCP data, a VHR DEM was generated. This DEM served as the 'ground truth' reference for subsequent comparisons and was also used to extract new secondary GCPs to improve the georeferencing of the satellite-derived DEMs.

To validate the accuracy of the satellite-derived DEMs, differences between models were assessed within specific measurement plots. These plots enabled calculation of the vertical offset of the satellite-derived DEMs compared to the UAV-derived DEM.

2.1. Study site

The study was conducted in the waste-dump area of a marble quarry located in Gummern, northwest of Villach in southern Austria (Fig. 2). The study site (including the waste dump and its surroundings) measures 68.63 ha. The waste-dump is in a mountainous region characterized by steep slopes, significant elevation changes, and dense beech and coniferous forests. Within the study area, extensive restoration and revegetation efforts have been implemented. The lower sections remain largely intact in their natural state, and the restoration process has progressed upwards in a tiered system, with access roads, used during the restoration works, separating each level. In the lower tiers, an advanced state of natural revegetation confirms the success of restoration activities.

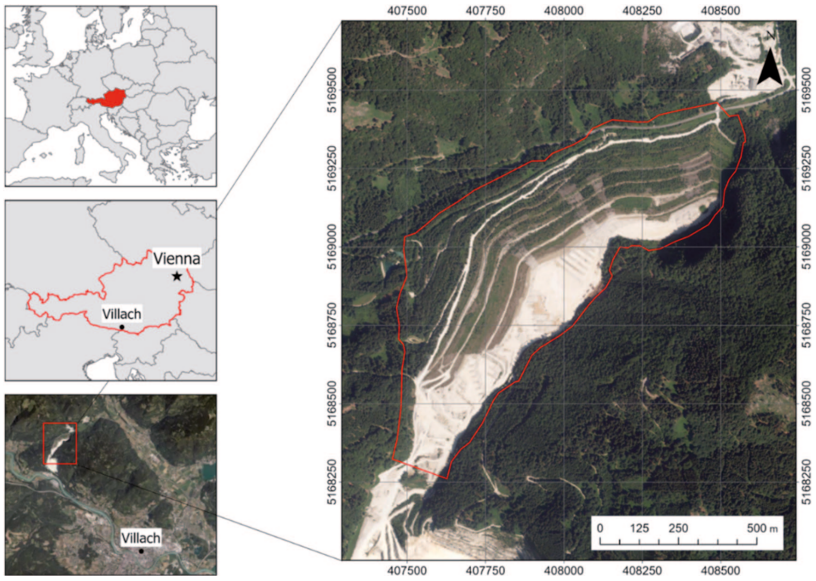

Fig. 2. Study area. Location of the marble quarry waste-dump in Gummern, northwest of Villach, Austria (coordinate reference system: EPSG25833)

2.2. Satellite imagery

Pléiades Neo, a constellation of four VHR satellites developed and operated by Airbus Defence and Space, was launched in pairs on 28 April 2021 and 16 August 2021. This constellation operates in a 700 km orbit with two orbital planes, allowing intra-day revisit times. The PleN sensor provides panchromatic images with a ground sampling distance (GSD) of 30 cm and multispectral images with a resolution of 1.20 m. The images used in this study were submetric-

resolution panchromatic images, extensively covering the quarry and its surroundings. Three images with different acquisition angles were used (TABLE 1).

TABLE 1

Pléiades Neo (PleN) tri-stereo image details (coordinate reference system: EPSG4258)

Image	1	2	3
Rows	37887	37409	37880
Columns	38965	38842	38861
Acquisition time	2023-10-02 T10:49:03.000Z	2023-10-02 T10:49:03.000Z	2023-10-02 T10:49:03.000Z
Northwest longitude (deg)	13.7167761	13.7169622	13.7163213
Northwest latitude (deg)	46.7101196	46.7105994	46.7125232
Southeast longitude (deg)	13.8706810	13.8707185	13.8719568
Southeast latitude (deg)	46.6080361	46.6081649	46.6071735

The WV2 satellite, launched by DigitalGlobe in October 2009, includes a panchromatic band with a spatial resolution of 0.50 m. A set of stereo images captured on 12 April 2024 were used (TABLE 2).

TABLE 2

WorldView-2 (WV2) stereo image details (coordinate reference system: EPSG4258)

Image	1	2
Rows	20120	20120
Columns	20943	20943
Acquisition time	2024-04-12T10:08:37.246120Z	2024-04-12T10:09:18.846073Z
Northwest longitude (deg)	13.73035022	13.73035022
Northwest latitude (deg)	46.70423254	46.70423254
Southeast longitude (deg)	13.86524609	13.86524609
Southeast latitude (deg)	46.61510588	46.61510588

2.3. UAV, camera, and flights

A series of UAV flights over the entire surface of the waste-dump captured multiple high-resolution aerial images, ensuring a high degree of overlap. This operation was carried out using the DJI Mavic 3M UAV, equipped with a 4/3-inch CMOS RGB sensor (20 MP resolution) and a multispectral camera system with four lenses capable of detecting wavelengths in the green, red, red-edge, and near-infrared (NIR) spectra. The RGB sensor had an 84° field of view (FOV), 24 mm equivalent focal length, f/2.8 to f/11 aperture, and an ISO range of 100-6400. Shutter speed was 8-1/8000 s for the electronic shutter, and 8-1/2000 s for the mechanical shutter, with a maximum image size of 5280x3956. The DJI Mavic 3M also features a real-time kinematics (RTK) module for centimetre-level positioning, essential for precision mapping.

Mission planning was done with the DJI Pilot 2 application. A surface of 53 ha, corresponding to the inside perimeter of the waste-dump, was covered by three flights, which lasted approximately 42 minutes each. The UAV flew at a constant height of 117 m above the terrain at a flight

speed of 5.1 m/s, resulting in a GSD of 5.4 cm. Flights were planned with 72% overlap and 65% sidelap. A total of 2,155 photos were taken, including the multispectral images. Due to varying lighting conditions in the study area during the flights (a mix of clouds and sun), exposure was set to automatic. Exposure times ranged from 1/500 s to 1/2000 s, with apertures between f/2.8 and f/4.5. ISO sensitivity varied from 100 to 420. The focal length remained fixed at 12 mm, with a maximum aperture of 2.97.

During the flights, the DJI D-RTK 2 High Precision GNSS Mobile Station, established as the RTK base station at one of the highest points of the waste-dump, offered specific root mean square (RMS) accuracy of 1 cm+1 ppm horizontally and 2 cm+1 ppm vertically in RTK FIX mode.

2.3.1. GCP establishment

Accurate georeferencing is a crucial component of aerial photogrammetry with drones, as it enables geographic coordinates to be accurately assigned to points in flight-captured images [27].

The first step was to establish GCPs to serve as known geographic references that would enhance and correct georeferencing accuracy. A total of 11 GCPs were established following a stratified distribution across the waste-dump levels, as this method has been demonstrated to produce small dispersion errors [28]. To ensure the points were easily identifiable in the UAV images, they were marked on the ground using a topographic aerosol paint (Fig. 3a).

Precise GCP coordinates were measured using a high-precision Carlson BRx7 GNSS receiver (Fig. 3b). Measurements, made using RTK connected to the Austrian Position Service (APOS) network via an NTRIP protocol, employed RTCM 3.2 and Virtual Reference Station (VRS). The coordinates were recorded with centimetre-level accuracy.

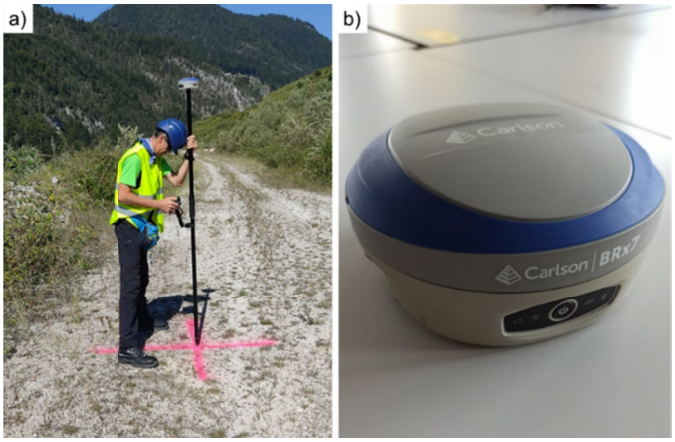

Fig. 3. Implementation of ground control points (GCP). Marking and measuring ground control points (a). Carlson BRx7 GNSS receiver (b)

2.3.2. SfM processing and DEM extraction

Since studies from various scientific fields support the reliability of Agisoft Metashape Professional (AMP) v.2.1.0 [29] in generating 3D models [30-33], this software was used for drone

flight image alignment and processing aimed at generating various photogrammetric products, including the DEM.

Images were aligned using the high accuracy option and the generic preselection option to reduce processing time. Following Sanz-Ablanedo et al. [27], 40,000 key point limits and 4,000 tie point limits per image were considered. Image alignment required 1 h 28 min of processing time, resulting in 1,241,016 tie points. All images (100%) were successfully aligned.

To perform the georeferencing, the GCPs were uploaded into the AMP project for automatic positioning based on their coordinates. To further improve georeferencing accuracy, manual repositioning was performed by aligning the GCPs with the painted ground markers observed in the images.

Subsequently, a dense point cloud was generated using the high accuracy and mild filtering modes. This process, which was completed in 2 h 16 min, resulted in a point cloud of nearly 279 million points, from which the DEM was derived, resulting in a raster file with a GSD of 5.73 cm.

2.4. Satellite imagery processing and georeferencing

To import the satellite images into the AMP project, it was necessary to first preprocesses them with the GDAL library [34], so as to convert the original PleN JPEG2000 image format to GeoTIFF with rational polynomial coefficient (RPC) metadata information. For WV2, the GDAL library was also necessary to combine all the image files in one single raster. From this point, SfM processing was as described in Section 2.3.2. Due to the great slopes in some areas of the quarry, empty gaps (blind spots) were evident on generating the high-quality dense point cloud. To fill these gaps, a medium-quality dense point cloud was also generated, which, thanks to the less restrictive parameters, showed no empty gaps. On merging both, the high-quality dense point cloud gaps were filled with the medium-quality dense point cloud data.

The RCP metadata-based georeferencing was found to be imprecise, as horizontal and vertical errors ranging from several to hundreds of metres were evident. Compared to the UAV-derived model, the PleN reconstruction exhibited horizontal displacement of over 700 m to the northwest and the WV2 model showed a much smaller offset of under 4 m in the same direction. These discrepancies rendered the satellite-derived DEMs unsuitable for direct application and measurement, as their geolocations did not align with the UAV-derived DEM. To accurately georeference the satellite-derived DEMs, 30 easily identifiable features – such as building corners, rocks, and other such distinctive objects – were selected in the 3D UAV DEM to serve as ground-truth references. These points were subsequently matched and transferred onto the satellite images (Fig. 4).

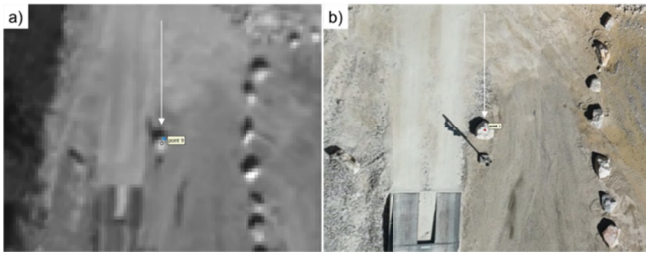

Fig. 4. Precise georeferencing of satellite imagery based on ground control points (GCPs). Coordinate extraction of recognizable points in satellite imagery (a) and unmanned aerial vehicle (UAV) digital elevation model (DEM) (b)

The pixel size of the UAV-derived DEM was also resampled, as the original pixel size of the drone model of 5.73 cm needed to be resampled to 30 cm and 50 cm to match the PleN DEM and WV2 DEM, respectively.

2.5. Volumetric and vertical accuracy calculations

Following a methodology similar to that of [5], to analyse altimetric discrepancies between the various DEMs, the UAV-derived DEM was subtracted from each satellite-derived DEM (PleN and WV2). Active areas of the waste-dump – showing variations due to time differences between image acquisition – are shown in Figs. 5a (PleN) and 5b (WV2).

In the non-active zones of the waste-dump area – where no significant visual changes were detected – 30 evenly distributed circular control plots were established (Fig. 5c), with diameters ranging from 5 m to 15 m. Within these plots, volumetric and altimetric differences between the DEMs were evaluated pixel by pixel. Calculated for each satellite-derived DEM were the mean altitude difference, root mean square error (RMSE), and standard deviation (SD) values. Additionally, cross-sectional profiles were extracted at three different locations (Fig. 5d) to visually illustrate the differences between the DEMs used in this study. Profiles 1 and 2 were located in areas affected by waste accumulation and were used to depict the topographic changes over time, whereas profile 3 was extracted from a non-variated area and served as a reference for assessing inter-dataset differences in stable terrain.

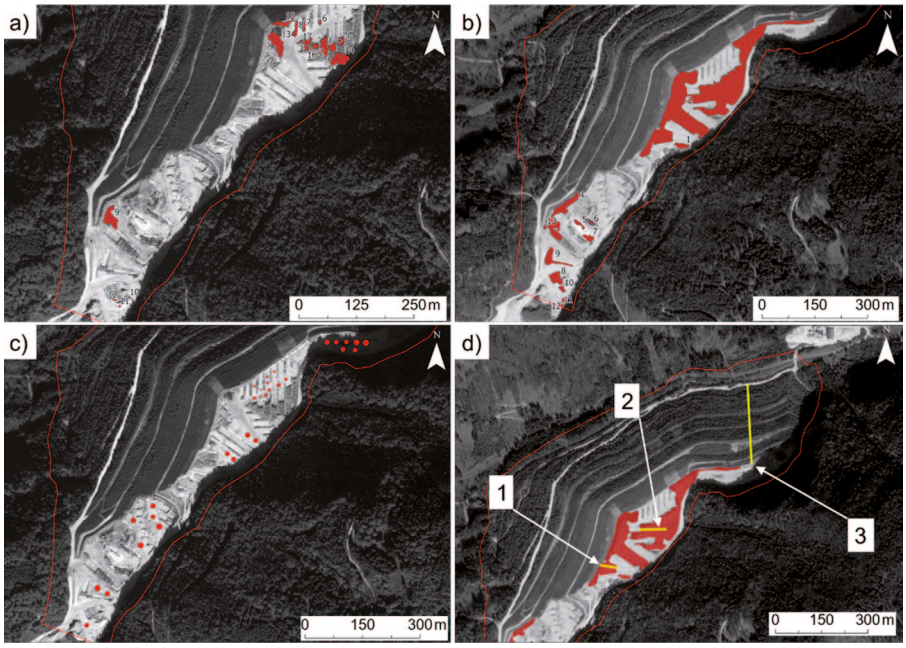

Fig. 5. Plots used for volume measurement for Pléiades Neo (PleN) tri-stereo (a) and WorldView-2 (WV2) (b), and reference plots located in non-variated areas as used for precision assessment (c). Location of the three cross-sectional profiles extracted at waste accumulation areas (profiles 1 and 2) and at non-variated area during the study period (profile 3) (d)

3. Results

The altitude differences observed between the PleN DEM and the UAV-derived DEM and between the WV2 DEM and UAV-derived DEM are depicted in Fig. 6. For both the PleN DEM (Fig. 6a) and WV2 DEM (Fig. 6b), areas with deposed and removed material were well identified at first sight. Note that horizontal banding in the PleN DEM generated the altimetric sinuosity evident in Fig. 6a (particularly in the southern half of the waste-dump), a phenomenon not observed in the WV2 DEM (Fig. 6b).

Non-disturbed vegetated surfaces, located principally in the northern and western areas of the study site, showed the highest altitude differences. The PleN DEM tended to overestimate

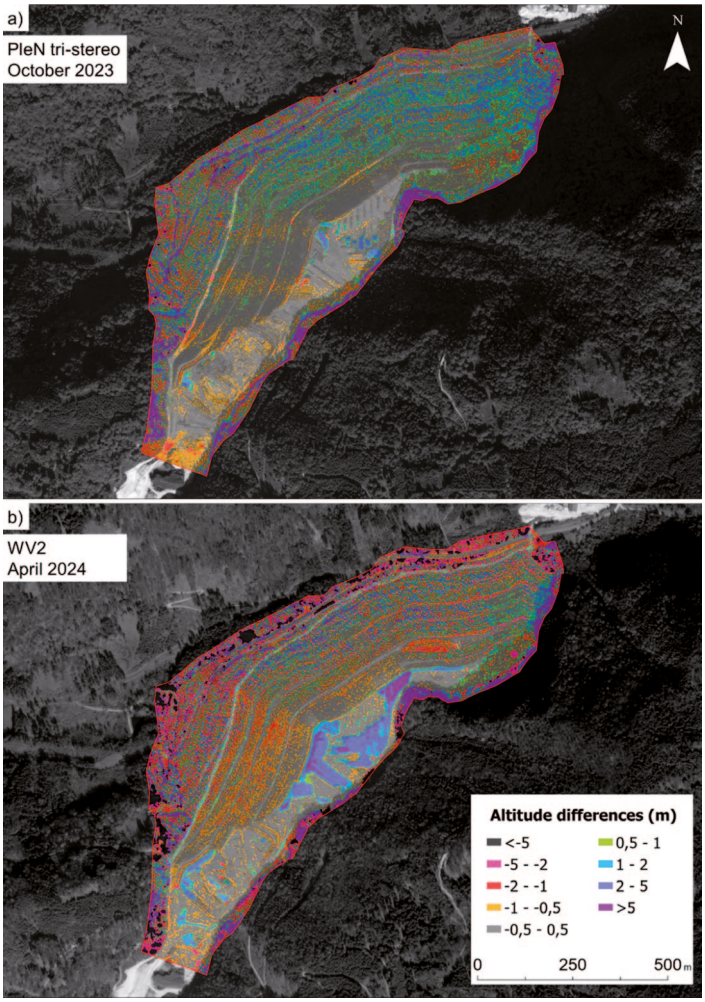

Fig. 6. Observed altitude differences (m) between the unmanned aerial vehicle (UAV) digital elevation model (DEM) from September 2023 and the Pléiades Neo (PleN) tri-stereo DEM from October 2023 (a) and the WorldView-2 (WV2) DEM from April 2024 (b)

vegetation height, with the greatest errors observed for mature vegetation and taller trees; smaller vegetation (shrubs and young trees) on the upper levels of the revegetated areas – principally on the west side – only showed differences of under 0.5 m/pixel. In contrast, the WV2 DEM tended to underestimate vegetation height, with the greatest errors likewise observed for taller vegetation. Levels of noise in shrubs and small vegetation were higher in the WV2 DEM compared to the PleN DEM. On comparing noise in the waste-dump active areas, both models presented broadly similar levels (slightly higher in the WV2 model), a fact that is more easily observed in the volume difference models (Fig. 7).

Regarding volume differences, the PleN DEM (Fig. 7a) presented values that did not exceed the range ±0.1 m^3/pixel in non-variated active waste-dump areas and small vegetation surfaces.

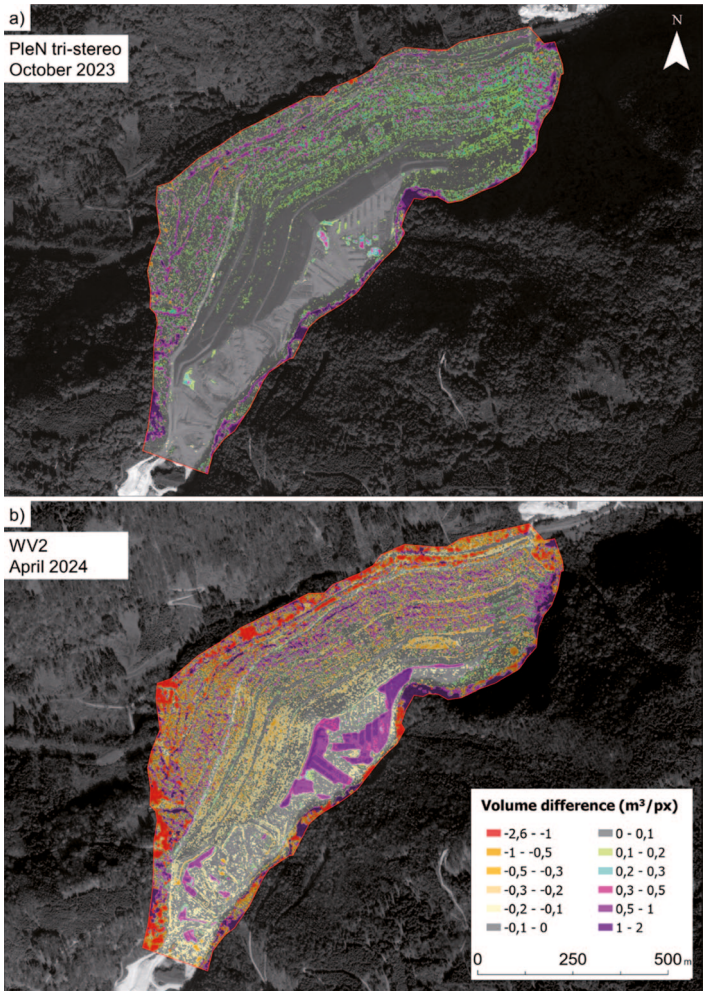

Fig. 7. Observed volume difference (m^3/pixel) between the unmanned aerial vehicle (UAV) digital elevation model (DEM) from September 2023 and the Pléiades Neo (PleN) tri-stereo DEM from October 2023 (a) and the WorldView-2 (WV2) DEM from April 2024 (b)

Deposed and removed material areas were easily identified at first sight. As with the altitude model, the greatest volume misassignments were observed for tall trees. Compared to the PleN DEM, the WV2 DEM (Fig. 7b) showed a slightly higher volume difference range in non-variated active waste-dump areas, with values in the range of ±0.3 m^3/pixel.

Focusing on the active waste-dump surface, satisfactory results were achieved for material movements throughout the temporal evolution of the waste-dump (Fig. 8). For PleN imagery, given that only one month had elapsed since the UAV flight, the amount of removed material was small (Fig. 8a). In contrast, for WV2 imagery, six months had passed, and consequently, major changes were evident in the waste-dump, which showed large surface area with deposed material (Fig. 8b).

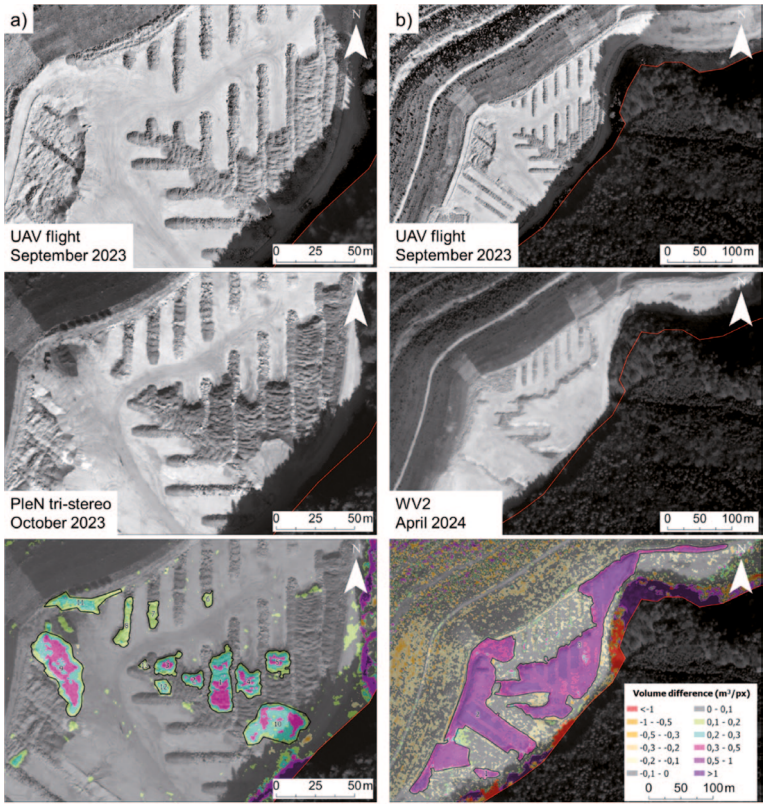

Fig. 8. Temporal evolution and detected volume differences for the period between the unmanned aerial vehicle (UAV) flight from September 2023 and the Pléiades Neo (PleN) tri-stereo imagery from October 2023 (a) and the WorldView-2 (WV2) imagery from April 2024 (b)

3.1. Volumetric and vertical accuracy results

According to the volume measurement plots, during the one-month period between the UAV flight and the PleN tri-stereo imagery, 11,310.3 m^3 of material was deposited, whereas only

74.6 m^3 was removed. In contrast, during the six-month period between the UAV flight and the WV2 imagery, 111,776.4 m^3 of material was deposed while 926.0 m^3 was removed.

Vertical accuracy assessments revealed an average vertical offset per pixel of –11.7 cm (RMSE = 24.8 cm) for the PleN tri-stereo height model and –18.6 cm (RMSE = 20.7 cm) for the WV2 height model. In bare terrain areas, the mean SD was ±22.6 cm for PleN and a slightly lower for WV2 (±17.9 cm), indicating a marginally better vertical consistency of the WV2-derived elevation model.

Cross-sectional profiles extracted at representative locations further illustrate both the temporal evolution of waste accumulation and the differences between the evaluated DEMs (Fig. 9). In profile 1, minor waste accumulation occurred between the UAV flight and the PleN

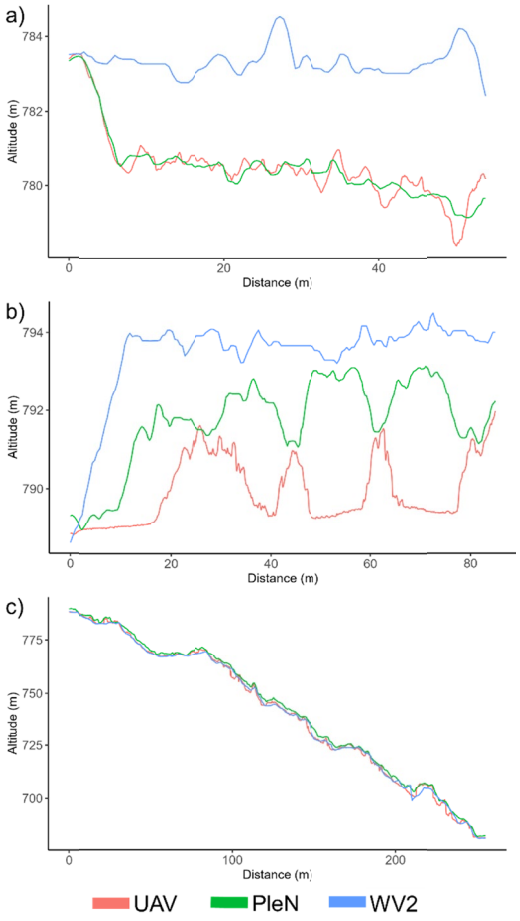

Fig. 9. Cross-sectional profiles derived from the UAV digital elevation model (DEM), the Pléiades Neo (PleN) tri-stereo DEM, and the Worldview-2 (WV2) DEM at different locations (Fig. 5d). Cross-sectional profile 1, where minor waste accumulation occurred between the UAV flight and the PleN imagery, whereas substantial waste accumulations occurred by the time WV2 imagery was acquired (a). Cross-sectional profile 2, where waste accumulation increased between the acquisition of the PleN and WV2 datasets (b). Cross-sectional profile 3, where no changes occurred during the study period (c)

imagery, whereas substantial waste accumulation was observed by the time the WV2 imagery was acquired. Profile 2, also located in an active deposition area, shows a clear increase in elevation between the PleN and WV2 datasets, consistent with the volumetric estimates. Conversely, profile 3, extracted from a non-varied area, exhibits a high degree of overlap among the three datasets, confirming the absence of significant topographic changes and supporting the reliability of the accuracy assessment.

A slight negative bias was consistently observed in the elevation difference distributions within the control plots for both the PleN and WV2 DEMs (Fig. 10), which is also reflected in the relative vertical offsets observed in the cross-sectional profiles.

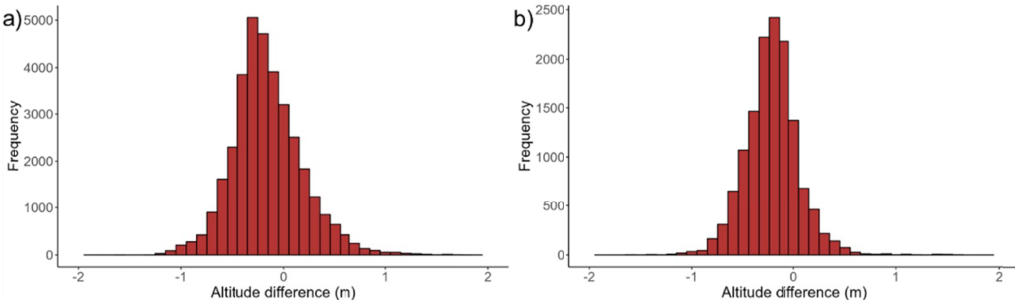

Fig. 10. Histogram showing the distribution of altitude differences in the control plots for Pléiades Neo (PleN) tri-stereo (a) and WorldView-2 (WV2) (b), showing a slight bias towards the negative side for both satellites compared to the unmanned aerial vehicle (UAV) model

4. Discussion

The monitoring of material movements in waste dumps has traditionally been addressed through field surveys and aircraft photogrammetric flights, and more recently, using UAV flights. While accuracy for field surveys is high, this approach is labour-intensive and time-consuming, leading to gradual disuse in recent decades, especially given the emergence of more efficient technologies. Aircraft photogrammetric flights, although effective, are costly and are typically only justified for large-scale projects or hazardous areas where ground access is challenging. UAVs, however, are a versatile and efficient tool for monitoring earth movements, with extensive scientific literature supporting their suitability for this task [15,35-37]. However, UAVs face certain limitations, such as reduced efficiency for large-scale areas, sensitivity to weather conditions [38], and regulatory flight restrictions in specific regions.

Regarding the use of satellite imagery, the existing literature is more limited. Traditionally, satellite imagery has been employed for automatic land-cover classification [39,40], thereby enabling analyses of mine surface expansion or reduction, changes in mining areas, and categorization of land cover over different time periods. The main obstacles to its application in volume measurements are the low spatial resolution of images and the limited accuracy of georeferenced data. Galchenko et al. [41], for instance, who used the conventional Sentinel-2 and Landsat 5-8 satellites to estimate mining waste volumes, reported constraint due to the relatively low spatial resolution of the images.

However, in the past decade, the scenario has changed significantly with the launch of VHR satellites. The PleN system enables the acquisition of tri-stereoscopic images with a panchromatic resolution of 30 cm, while WV2 offers resolutions of 50 cm. Other satellites, such as IKONOS and QuickBird, have also contributed to this evolution, although the application of VHR imagery remains limited due to the hardware requirements for processing this data [42]. Nonetheless, advances in photogrammetric techniques, e.g., SfM, have significantly simplified image processing, enabling the generation of high-resolution DEMs using more accessible and user-friendly software [43]. Additionally, the acquisition of satellite imagery has become more feasible with the increasing availability of commercial platforms like Maxar and Planet providing access to VHR data. However, note that the high cost of these images may limit their use in smaller-scale projects.

To optimize the process of obtaining high-resolution DEMs, this study has proposed a combined approach that integrates various geomatics tools. Periodic use is made of satellite imagery, which is precisely georeferenced using a very high-resolution UAV-derived DEM and GCPs acquired by precision GNSS receivers. In our approach, high-resolution DEMs generated with UAVs and obtained occasionally (e.g., every two to three years) serve as a reference for georeferencing DEMs derived from satellite imagery. These satellite-derived DEMs can be acquired more frequently without additional fieldwork, thereby enhancing efficiency in long-term monitoring projects.

The proposed methodology was tested, validated, and evaluated at a pilot site, with very satisfactory results. Compared to the reference UAV-derived DEM, the DEMs generated from PleN and WV2 images exhibited an average height difference of 24.8 cm (RMSE) and 20.7 cm (RMSE), respectively. Additionally, SD values were 22.6 cm and 17.9 cm for PleN and WV2, respectively. Our results are consistent with those reported by other authors. Hu et al. [44], who assessed elevation biases for WV3 in a mountainous region, reported an SD of 62 cm compared to an airborne high-precision LiDAR point cloud, while Aguilar et al. [45], who evaluated vertical accuracy for WV2 and WV3 satellites relative to LiDAR, obtained SD values of 26 cm and 20 cm, respectively.

While most previous studies have relied on LiDAR as ground-truth data [25,26,44-47], a novelty of our study was the use of SfM drone data as a reference for evaluating the vertical accuracy of VHR satellite imagery in volume measurements. Our study, in demonstrating the potential of SfM photogrammetry for accurately georeferencing satellite DEMs, offers a cost-effective and time-efficient alternative to LiDAR [48,49].

In analysing height differences across the entire surface, the greatest discrepancies were detected in wooded areas, with values exceeding 5 m in some cases. Interestingly, errors were observed principally in gaps between trees, while canopy tops appeared to be accurately represented in the satellite models. This discrepancy can be attributed to spatial resolution differences between the UAV DEM and satellite DEMs. In densely vegetated areas, the higher resolution of UAV imagery enabled gaps to be detected between trees, meaning that the drone point cloud achieved surface values even in dense forest areas. However, when the UAV model was resampled to match the resolution of the satellite models, the resulting pixel values included both terrain and canopy heights. Consequently, since ground-level gaps were included, the average height of the resampled pixels was lower than the actual canopy height. In contrast, satellite models captured only the canopy tops. These altimetric differences were especially evident in shadowed surfaces, where ±20 m differences were observed. This effect was also observed by Gong and Fritsch [50], who reported height errors exceeding 15 m in shadowed areas during digital reconstructions.

Pléiades Neo exhibited a tendency to overestimate vegetation height, whereas discrepancies for low, spare shrub vegetation were minimal. Altitude errors were also minimal in active mining waste-dump areas with bare and flat terrain. However, as previously documented by Loghin et al. [25,47] for the original Pléiades tri-stereo constellation, a banding effect was observed in the PleN DEM, appearing to be a systematic error. In contrast, WV2 tended to underestimate vegetation height and showed discrepancies in shrub-covered areas. However, in bare waste-dump terrain, the WV2 model performed well, albeit with a slightly granular appearance compared to the PleN model.

In any case, the achieved vertical offsets (–11.7 cm and –18.6 cm for PleN and WV2, respectively) are comparable with previous reports of volumetric stockpile measurements performed with drones. Filkin et al. [15] reported RMSE values ranging from 16.1 cm to 4.3 cm depending on drone type and GCP distribution; Ren et al. [51], who analysed the influence of GCP number and placement, obtained RMSE values of 36.6 cm to 5.3 cm; and Mello et al. [52], who performed multitemporal landfill volumetric measurements, reported a maximum vertical error of 37 cm. These comparisons highlight the satisfactory accuracy of VHR satellite-derived models, despite the inherent spatial resolution differences between drone and satellite imagery.

Very high-resolution satellites show great promise for mining waste-dump volume estimation purposes. In our study, the vertical accuracies achieved for PleN and WV2 with the proposed integration of various geomatics tools confirm the capability of these sensors to generate reliable DEMs that can be translated into volumetric maps. Integrating this approach with a multitemporal analysis means that mining waste material movements can be effectively monitored, reducing fieldwork, effort, and cost.

5. Conclusions

Very high-resolution satellites such as PleN tri-stereo and WV2 are highly effective for photogrammetric projects. In our study, very satisfactory results were obtained for both terrain modelling and volumetric analysis compared to results for high-resolution DEMs generated using UAV imagery. The UAV-based model, in combination with GNSS GCPs, allowed for accurate georeferencing of the satellite-derived DEMs. A slight banding effect observed in the PleN DEM was likely caused by the sensor's internal construction rather than by errors in the model generation process.

The PleN (30 cm) and WV2 (50 cm) images proved to be highly effective in detecting and monitoring mining waste-dump variations. The main limitations of VHR DEMs were observed for tall dense tree surfaces, where significant discrepancies emerged compared to the UAV model. This can be attributed to pixel size differences between the drone and satellite sensors. The gaps between trees were captured by the UAV due to higher spatial resolution of the UAV images compared to the satellite images, leading to discrepancies in vegetated areas. However, the height estimates of the tree canopy tops remained consistent and reliable.

The use of VHR satellite imagery presents numerous possibilities for monitoring and assessing mining activities and natural resources. Future research could focus on multitemporal analysis of mining waste expansion in recent years and the verification of compliance with environmental regulations.

Acknowledgements

This study is funded by the European Union under grant agreement no. 101091616, project S34I – SECURE AND SUSTAINABLE SUPPLY OF RAW MATERIALS FOR EU INDUSTRY, coordinated by Ana C. Teodoro. Iván González-Pérez gratefully acknowledges the financial support provided by the Consejería de Educación de la Junta de Castilla y León and the European Social Fund Plus (grants for pre-doctoral research 2025).

References

[1] M. Lazăr, I.-M. Nyari, F.G. Faur, Methodology for assessing the environmental risk due to mining waste dumps sliding – case of study of Jiu Valley. Carpathian J. Earth Environ. Sci. **10** (2015).

[2] N. Adibee, M. Osanloo, M. Rahmanpour, Adverse effects of coal mine waste dumps on the environment and their management. Environ. Earth Sci. **70**, 1581-1592 (2013). DOI: https://doi.org/10.1007/s12665-013-2243-0

[3] M.A. Pashkevich, Chapter 1 – Classification and Environmental Impact of Mine Dumps. In: J. Bech, C. Bini, M.A. Pashkevich (Eds.), Assessment, Restoration and Reclamation of Mining Influenced Soils, Academic Press, pp. 1-32 (2017). DOI: https://doi.org/10.1016/B978-0-12-809588-1.00001-3

[4] G. Žibret, M. Gosar, M. Miler, J. Alijagić, Impacts of mining and smelting activities on environment and landscape degradation – Slovenian case studies. Land Degrad. Develop. **29**, 4457-4470 (2018). DOI: https://doi.org/10.1002/ldr.3198

[5] A.S. Louw, R. Avtar, Methodology for measuring landfill dumping statistics globally using Digital Elevation Change maps. Resour. Conserv. Recycl. **212**, 107924 (2025). DOI: https://doi.org/10.1016/j.resconrec.2024.107924

[6] I. Atif, H. Ashraf, F.T. Cawood, M.A. Mahboob, A Conceptual Digital Framework for Near Real-Time Monitoring and Management of Mine Tailing Storage Facilities. In: X.-N. Bui, C. Lee, C. Drebenstedt (Eds.), Proc. Int. Conf. Innov. Sustain. Responsible Mining, Springer Int. Publ., Cham, pp. 498-530 (2021). DOI: https://doi.org/10.1007/978-3-030-60839-2_27

[7] A. Soofastaei, Mines and Machines: Virtual Assistants in Modern Mining. In: Advanced Virtual Assistants – A Window to the Virtual Future. IntechOpen (2024). DOI: https://doi.org/10.5772/intechopen.1003846

[8] B. Kršák, P. Blišťan, A. Pauliková, P. Puškárová, Ľ. Kovanič, J. Palková, V. Zelizňaková, Use of low-cost UAV photogrammetry to analyze the accuracy of a digital elevation model in a case study. Measurement **91**, 276-287 (2016). DOI: https://doi.org/10.1016/j.measurement.2016.05.028

[9] I.N.S. Parwata, S. Nakashima, N. Shimizu, T. Osawa, Effect of digital elevation models on monitoring slope displacements in open-pit mine by differential interferometry synthetic aperture radar. J. Rock Mech. Geotech. Eng. **12**, 1001-1013 (2020). DOI: https://doi.org/10.1016/j.jrmge.2020.01.003

[10] G.J.J. Verhoeven, Providing an archaeological bird's-eye view – an overall picture of ground-based means to execute low-altitude aerial photography (LAAP) in Archaeology. Archaeol. Prospect. **16**, 233-249 (2009). DOI: https://doi.org/10.1002/arp.354

[11] Q. Guo, H. Liu, F.M. Hassan, M.W. Bhatt, A.M. Buttar, Application of UAV tilt photogrammetry in 3D modeling of ancient buildings. Int. J. Syst. Assur. Eng. Manag. **13**, 424-436 (2022). DOI: https://doi.org/10.1007/s13198-021-01458-4

[12] N. Snavely, S.M. Seitz, R. Szeliski, Modeling the World from Internet Photo Collections. Int. J. Comput. Vis. **80**, 189-210 (2008). DOI: https://doi.org/10.1007/s11263-007-0107-3

[13] D. Zekkos, W. Greenwood, J. Lynch, J. Manousakis, A. Athanasopoulos-Zekkos, M. Clark, K.L. Cook, C. Saroglou, Lessons Learned from the Application of UAV-Enabled Structure-From-Motion Photogrammetry in Geotechnical Engineering. ISSMGE Int. J. Geoeng. Case Hist. **4**, 254-274 (2018). DOI: https://doi.org/10.4417/IJGCH-04-04-03

[14] G. Rock, J.B. Ries, T. Udelhoven, Sensitivity analysis of UAV-photogrammetry for creating digital elevation models (DEM). ISPRS Arch. **XXXVIII-1-C22**, 69-73 (2012). DOI: https://doi.org/10.5194/isprsarchives-XXXVIII-1-C22-69-2011

[15] T. Filkin, N. Sliusar, M. Huber-Humer, M. Ritzkowski, V. Korotaev, Estimation of dump and landfill waste volumes using unmanned aerial systems. Waste Manag. **139**, 301-308 (2022). DOI: https://doi.org/10.1016/j.wasman.2021.12.029

[16] O.G. Ajayi, A.A. Salubi, A.F. Angbas, M.G. Odigure, Generation of accurate digital elevation models from UAV acquired low percentage overlapping images. Int. J. Remote Sens. **38**, 3113-3134 (2017). DOI: https://doi.org/10.1080/01431161.2017.1285085

[17] S. Coveney, K. Roberts, Lightweight UAV digital elevation models and orthoimagery for environmental applications: data accuracy evaluation and potential for river flood risk modelling. Int. J. Remote Sens. **38**, 3159-3180 (2017). DOI: https://doi.org/10.1080/01431161.2017.1292074

[18] L. Hashemi-Beni, J. Jones, G. Thompson, C. Johnson, A. Gebrehiwot, Challenges and Opportunities for UAV-Based Digital Elevation Model Generation for Flood-Risk Management: A Case of Princeville, North Carolina. Sensors **18**, 3843 (2018). DOI: https://doi.org/10.3390/s18113843

[19] D. Moravec, J. Komarek, J. Kumhálová, M. Kroulik, J. Prošek, P. Klápště, Digital elevation models as predictors of yield: Comparison of an UAV and other elevation data sources. Agron. Res. **15**, 249-255 (2017).

[20] D.E. Shean, O. Alexandrov, Z.M. Moratto, B.E. Smith, I.R. Joughin, C. Porter, P. Morin, An automated, open-source pipeline for mass production of digital elevation models (DEMs) from very-high-resolution commercial stereo satellite imagery. ISPRS J. Photogramm. Remote Sens. **116**, 101-117 (2016). DOI: https://doi.org/10.1016/j.isprsjprs.2016.03.012

[21] S. Wang, Z. Ren, C. Wu, Q. Lei, W. Gong, Q. Ou, H. Zhang, G. Ren, C. Li, DEM generation from Worldview-2 stereo imagery and vertical accuracy assessment for its application in active tectonics. Geomorphology **336**, 107-118 (2019). DOI: https://doi.org/10.1016/j.geomorph.2019.03.016

[22] M. Bagnardi, P.J. González, A. Hooper, High-resolution digital elevation model from tri-stereo Pleiades-1 satellite imagery for lava flow volume estimates at Fogo Volcano. Geophys. Res. Lett. **43**, 6267-6275 (2016). DOI: https://doi.org/10.1002/2016GL069457

[23] A. Nemmaoui, F.J. Aguilar, M.A. Aguilar, R. Qin, DSM and DTM generation from VHR satellite stereo imagery over plastic covered greenhouse areas. Comput. Electron. Agric. **164**, 104903 (2019). DOI: https://doi.org/10.1016/j.compag.2019.104903

[24] D.J. Backes, F.N. Teferle, Multiscale Integration of High-Resolution Spaceborne and Drone-Based Imagery for a High-Accuracy Digital Elevation Model Over Tristan da Cunha. Front. Earth Sci. **8**, (2020). DOI: https://doi.org/10.3389/feart.2020.00319

[25] A.-M. Loghin, J. Otepka-Schremmer, W. Karel, M. Pöchtrager, N. Pfeifer, Accuracy Analysis of Digital Elevation Models from very High Resolution Satellite Imagery, presented at the Dreiländertagung der OVG, DGPF und SGPF: Photogrammetrie – Fernerkundung – Geoinformation – 2019, Publikationen der DGPF, pp. 123-137 (2019).

[26] Y. Zhou, B. Parsons, J.R. Elliott, I. Barisin, R.T. Walker, Assessing the ability of Pleiades stereo imagery to determine height changes in earthquakes: A case study for the El Mayor-Cucapah epicentral area. J. Geophys. Res.: Solid Earth **120**, 8793-8808 (2015). DOI: https://doi.org/10.1002/2015JB012358

[27] E. Sanz-Ablanedo, J.H. Chandler, J.R. Rodríguez-Pérez, C. Ordóñez, Accuracy of Unmanned Aerial Vehicle (UAV) and SfM Photogrammetry Survey as a Function of the Number and Location of Ground Control Points Used. Remote Sens. **10**, 1606 (2018). DOI: https://doi.org/10.3390/rs10101606

[28] C. Cabo, E. Sanz-Ablanedo, J. Roca-Pardiñas, C. Ordóñez, Influence of the Number and Spatial Distribution of Ground Control Points in the Accuracy of UAV-SfM DEMs: An Approach Based on Generalized Additive Models. IEEE Trans. Geosci. Remote Sens. **59**, 10618-10627 (2021). DOI: https://doi.org/10.1109/TGRS.2021.3050693

[29] https://www.agisoft.com/features/professional-edition/, accessed: 17.02.2025

[30] K. Themistocleous, A. Agapiou, G. Papadavid, M. Christoforou, D.G. Hadjimitsis, The use of UAV to document sloping landscapes to produce digital elevation models to examine environmental degradation, in: Earth Resources and Environmental Remote Sensing/GIS Applications VI. SPIE, pp. 118-126 (2015). DOI: https://doi.org/10.1117/12.2195623

[31] J. Chen, K. Clarke, Rapid 3D modeling using photogrammetry applied to Google Earth. (2016).

[32] K.H.Z.K.Z. Abidin, M.A.M. Razi, S.M. Bukari, Analysis the Accuracy of Digital Elevation Model (DEM) for Flood Modelling on Lowland Area. IOP Conf. Ser.: Earth Environ. Sci. **140**, 012014. (2018). DOI: https://doi.org/10.1088/1755-1315/140/1/012014

[33] A. Jebur, F. Abed, M. Mohammed, Assessing the performance of commercial Agisoft PhotoScan software to deliver reliable data for accurate 3D modelling. MATEC Web Conf. **162**, 03022 (2018). DOI: https://doi.org/10.1051/matecconf/201816203022

[34] E. Rouault, F. Warmerdam, K. Schwehr, A. Kiselev, H. Butler, M. Łoskot, T. Szekeres, E. Tourigny, M. Landa, I. Miara, B. Elliston, K. Chaitanya, L. Plesea, D. Morissette, A. Jolma, N. Dawson, D. Baston, C. de Stigter, H. Miura, GDAL (2025). DOI: https://doi.org/10.5281/zenodo.5884351

[35] S. Mantey, M.S. Aduah, Comparative Analysis of Stockpile Volume Estimation using UAV and GPS Techniques. Ghana Min. J. **21**, 1-10 (2021). DOI: https://doi.org/10.4314/gm.v21i1.1

[36] G. Yüksel, A. Ulvi, M. Yakar, Usage of unmanned aerial vehicles in open mine sites. Intercont. Geoinf. Days **4**, 13-16 (2022).

[37] G. Saratsis, G. Xiroudakis, G. Exadaktylos, A. Papaconstantinou, I. Lazos, Use of UAV Images in 3D Modelling of Waste Material Stock-Piles in an Abandoned Mixed Sulphide Mine in Mathiatis – Cyprus. Mining **3**, 79-95 (2023). DOI: https://doi.org/10.3390/mining3010005

[38] K. Johnson, E. Nissen, S. Saripalli, J.R. Arrowsmith, P. McGarey, K. Scharer, P. Williams, K. Blisniuk, Rapid mapping of ultrafine fault zone topography with structure from motion. Geosphere **10**, 969-986 (2014). DOI: https://doi.org/10.1130/ges01017.1

[39] R. Ahumada-Mexía, J.M. Murillo-Jiménez, A. Ortega-Rubio, A.J. Marmolejo-Rodríguez, E.H. Nava-Sánchez, Identification of mining waste using remote sensing technique: A case study in El Triunfo town, BCS, México. Remote Sens. Appl.: Soc. Environ. **22**, 100493 (2021). DOI: https://doi.org/10.1016/j.rsase.2021.100493

[40] M. Silva, G. Hermosilla, G. Villavicencio, P. Breul, Automated Detection and Analysis of Massive Mining Waste Deposits Using Sentinel-2 Satellite Imagery and Artificial Intelligence. Remote Sens. **15**, 4949 (2023). DOI: https://doi.org/10.3390/rs15204949

[41] Y.P. Galchenko, Y.A. Ozaryan, T.V. Kozhevnikova, V.E. Okladnikov, Identification of Mining Waste Disposal Facilities Using Remote Sensing Data. J. Min. Sci. **60**, 688-694 (2024). DOI: https://doi.org/10.1134/S106273912404015X

[42] S. Jiang, Y. Tarabalka, W. Yao, Z. Hong, G. Feng, Space-to-speed architecture supporting acceleration on VHR image processing. ISPRS J. Photogramm. Remote Sens. **198**, 30-44 (2023). DOI: https://doi.org/10.1016/j.isprsjprs.2023.02.010

[43] A.R. Mosbrucker, J.J. Major, K.R. Spicer, J. Pitlick, Camera system considerations for geomorphic applications of SfM photogrammetry. Earth Surf. Process. Landforms **42**, 969-986 (2017). DOI: https://doi.org/10.1002/esp.4066

[44] F. Hu, X.M. Gao, G.Y. Li, M. Li, DEM extraction from WorldView-3 stereo-images and accuracy evaluation. ISPRS Arch. **XLI-B1**, 327–332 (2016). DOI: https://doi.org/10.5194/isprs-archives-XLI-B1-327-2016

[45] M.A. Aguilar, A. Nemmaoui, F.J. Aguilar, R. Qin, Quality assessment of digital surface models extracted from WorldView-2 and WorldView-3 stereo pairs over different land covers. GISci. Remote Sens. **56**, 109-129 (2019). DOI: https://doi.org/10.1080/15481603.2018.1494408

[46] E. Mandanici, V.A. Girelli, L. Poluzzi, Metric Accuracy of Digital Elevation Models from WorldView-3 Stereo-Pairs in Urban Areas. Remote Sens. **11**, 878 (2019). DOI: https://doi.org/10.3390/rs11070878

[47] A.-M. Loghin, J. Otepka-Schremmer, C. Ressl, N. Pfeifer, Improvement of VHR Satellite Image Geometry with High Resolution Elevation Models. Remote Sens. **14**, 2303 (2022). DOI: https://doi.org/10.3390/rs14102303

[48] C. Stone, M. Webster, J. Osborn, I. Iqbal, Alternatives to LiDAR-derived canopy height models for softwood plantations: a review and example using photogrammetry. Aust. For. **79**, 271-282 (2016). DOI: https://doi.org/10.1080/00049158.2016.1241134

[49] F. Chiabrando, A. Spanò, G. Sammartano, L.T. Losè, UAV oblique photogrammetry and lidar data acquisition for 3D documentation of the Hercules Fountain. Virtual Archaeol. Rev. **8**, 83-96 (2017). DOI: https://doi.org/10.4995/var.2017.5961

[50] K. Gong, D. Fritsch, A detailed study about digital surface model generation using high resolution satellite stereo imagery. ISPRS Ann. Photogramm. Remote Sens. Spatial Inf. Sci. **III-1**, 69-76 (2016). DOI: https://doi.org/10.5194/isprs-annals-III-1-69-2016

[51] H. Ren, Y. Zhao, W. Xiao, X. Wang, T. Sui, An Improved Ground Control Point Configuration for Digital Surface Model Construction in a Coal Waste Dump Using an Unmanned Aerial Vehicle System. Remote Sens. **12**, 1623 (2020). DOI: https://doi.org/10.3390/rs12101623

[52] C.C. de S. Mello, D.H.C. Salim, G.F. Simões, UAV-based landfill operation monitoring: A year of volume and topographic measurements. Waste Manag. **137**, 253-263 (2022). DOI: https://doi.org/10.1016/j.wasman.2021.11.020